Biosynthesis of SiO2 nanoparticles using extract of Nerium oleander leaves for the removal of tetracycline antibiotic

Noureddine El Messaoudi, Mohammed El Khomri, El-Houssaine Ablouh, Amal Bouich, Abdellah Lacherai, Amane Jada, Eder Lima, Farooq Sher

Chemosphere, Volume287, Article Number132453, JANUARY 2022

DOI10.1016/j.chemosphere.2021.132453

Biosynthesis of SiO2 nanoparticles using extract of Nerium oleander leaves for the removal of tetracycline antibiotic

El Messaoudi, N[1] ; El Khomri, M[1] ; Ablouh, EH[2] ; Bouich, A[3]; Lacherai, A[1]; Jada, A[4]; Lima, EC[5] ; Sher, F[6]

[1] Ibn Zohr Univ, Lab Appl Chem & Environm, Agadir 80000, Morocco
[2] Mohammed VI Polytech Univ UM6P, Mat Sci Energy & Nanoengn Dept MSN, Benguerir 43150, Morocco
[3] Univ Politecn Valencia, Inst Design & Mfg IDF, Dept Appl Phys, Valencia 46000, Spain
[4] High Alsace Univ, Inst Mat Sci Mulhouse IS2M, F-68100 Mulhouse, France
[5] Fed Univ Rio Grande do Sul UFRGS, Inst Chem, BR-91501970 Porto Alegre, RS, Brazil

Abstract

The present study aims to improve the adsorption of tetracycline (TC) antibiotic onto dioxide silicon nanoparticles (SiO_2 NPs) biosynthesized from the extract of *Nerium oleander* leaves. The SiO_2 NPs were characterized using SEM-EDX, BET-BJH, FTIR-ATR, TEM, and XRD. TC adsorption on SiO_2 NPs followed the pseudo 2nd order model and the Langmuir isotherm model with *Qm* was 552.48 mg g^{-1}. The removal of TC using SiO_2 NPs was 99.56 % at conditions (SiO_2 NPs amount=0.25 g L^{-1}, C_0=25 mg L^{-1}, and t=40 min) based on design-optimization. Electrostatic interaction governs the adsorption mechanism is attributed. The reusability of SiO_2 NPs was tested, and the performance adsorption was 85.36 % after the five cycles. The synthesized SiO_2 NPs as promising adsorbent has a potential application for antibiotics removal from wastewaters.

Keywords: Tetracycline antibiotic; SiO_2 nanoparticles; *Nerium oleander* leaves adsorption; optimization; wastewater treatment

1 Introduction

One of the major pollutants in wastewater is antibiotics. Various antibiotics such as quinolones, sulfonamides, macrolides, and tetracyclines are broadly used to prevent and treat infectious diseases (Ahamad et al., 2019). Tetracycline (TC) is commonly used for animal husbandry and poultry industries worldwide to promote animal growth and prevent diseases (Aalipour et al., 2014; Song et al., 2020; Van et al., 2020). About 60-80 % of tetracyclines were subject to different natural surroundings original in or metabolized forms due to lower metabolic rates in animals and humans (Epps and Blaney, 2016; Scaria et al., 2021). Due to the high solubility rate, TC is detected in different water bodies and some regions; its concentration exceeds standard environmental limits (Daghrir and Drogui, 2013). Antibiotic residues, frequently found in soil, sediment, and aquatic environments, have adverse side effects as bacterial resistance changes in the microbial ecological functions (Grenni et al., 2018; Sodhi et al., 2021). Antibiotic accumulation may also severely impair human physiological functions and have carcinogenic, teratogenic, or hormonal effects (Liu et al., 2017; Yu et al., 2016), their excess entrance into food chains may cause different disorders in the human body such as gastrointestinal system (Rashidi Nodeh et al., 2020). Therefore, controlling and handling antibiotic contaminants is necessary to have a safe environment.

Several approaches such as membrane filtration, photocatalysis, flocculation, biological treatment, electrochemical, adsorption, and reverse osmosis have been used to remove antibiotics from wastewaters (Rostam and Taghizadeh, 2020; Sharma et al., 2020; Wang et al., 2021). Among these methods, the adsorption process is competitive, high efficiency, low energy demand, and the possibility of reusing adsorbent materials (El Khomri et al., 2020; El Messaoudi et al., 2016a).

Many materials have been used as adsorbents materials, including nanoparticles (MgO, CuO, TiO_2, ZnO, SiO_2, etc.) due to their high-performance adsorption (Das et al., 2017; Ibrahim et al., 2016; Li et al., 2021). Still, the efficacy of SiO_2 is proved to be better due to its unique conductive nature. SiO_2 nanoparticles are used as an excellent adsorbent for the removal of dyes and metals, and a photocatalyst to treat wastewaters (Chen et al., 2012; Hosseini et al., 2018; Sharma et al., 2021). The biosynthesis of nanoparticles from the extract of agricultural solid wastes is regarded as a simple, rapid, cost-effective, and eco-friendly method for creating nanostructured materials such as metals, metal chalcogenides, and bimetal oxide (Das et al., 2018). In this work, we used an extract of *Nerium oleander* leaves for biosynthesized of SiO_2. The *Nerium oleander* leave is agricultural solid waste used for pollutants removal in some studies, but its performance as an adsorbent was limited because of its undeveloped porous structure (Martín et al., 2018; Sebeia et al., 2019; Suba et al., 2018).

The performance of SiO_2 NPs was evaluated in this study by removing tetracycline from the solution aqueous. Besides, characterization techniques were practiced for investigating its structure and properties, such as scanning electron microscope coupled with energy-dispersive X-ray (SEM-EDX), Brunauer-Emmett-Teller and Barrett-Joyner-Halenda (BET-BJH), Fourier transform infrared spectroscopy coupled with attenuated total reflectance (FTIR-ATR), transition electron microscope (TEM), X-ray diffraction (XRD), and point of zero charge (PZC). The present work will substantially impact as it will add unique knowledge on the adsorption potential of SiO_2 NPs synthesized from the extract of *Nerium oleander* leaves. In this current study, the SiO_2 NPs were synthesized from the *Nerium oleander* leaves extract. The impact of different influencing experimental parameters such as pH, SiO_2 NPs dose, reaction time, and TC concentration was investigated. Kinetic and equilibrium models evaluated the adsorption of TC on SiO2 NPs. The removal of TC optimized using Box–Behnken design (BBD). The adsorption mechanism of TC molecules on

74 the SiO_2 NPs surface was proposed. The reusability of SiO_2 NPs was evaluated.

75 2 Experimental

76 2.1 Materials

77 *Nerium oleander* leaves were collected in Tinghir (South-East Morocco). The silicate of
78 sodium (Na_2SiO_3), tetracycline (antibiotic, $C_{22}H_{24}N_2O_8$, MW=444.435 g mol^{-1}), C_2H_5OH,
79 HCl, and NaOH were parched from Sigma-Aldrich. The distilled and deionized waters were
80 used through experiments.

81 2.2 Biosynthesis SiO_2 NPs

82 10 g *Nerium oleander* leave powder were added in 100 mL of C_2H_5OH and stirred for 3h.
83 After that, the solution was filtered using filter paper then the above mixture was centrifuged
84 for obtained a clear extract of *Nerium oleander* leaves. 2 g Na_2SiO_3 and 50 mL of extract and
85 5 mL of NaOH (0.5 M) were mixed and stirred for 4h. After precipitation, the mixture was
86 filtered and centrifuged for separated the liquid and the precipitate (SiO_2 NPs). The residue
87 obtained was watched with deionized water. Finally, The SiO_2 nanoparticles were over-dried
88 (80 °C) for 24 h and calcined in the furnace at 500 °C for 3 h.

89 2.3 Characterization

90 The physicochemical properties of SiO_2 NPs were examined using different characterization
91 techniques. The morphology and microstructures of SiO_2 NPs were examined by SEM-EDX
92 analysis (JEOL, JSM-IT200) and TEM analysis (Philips CM-30). BET and BJH methods
93 (Belsorp Mini II) were used to determine the surface area, total pore volume, and diameter
94 pore of SiO_2 NPs. The chemical bond characteristics of SiO_2 NPs before and after TC
95 adsorption was acquired by FTIR-ATR analysis (Jasco 4100). The SiO_2 NPs crystal structures
96 were evaluated using XRD analysis recorded on a 6100-Shimadzu. The PZC of adsorbent was
97 determined using the method reported by Fiol and Villaescusa, (2009).

2.4 Batch adsorption experiments

The TC adsorption onto SiO_2 NPs nanoparticles was conducted in batch mode using 12.5 mg of SiO_2 NPs in 50 mL of TC solutions with concentrations varied from 50 to 200 mg L^{-1} at 23±1°C. The influence of pH solution on adsorption was assessed and varied from 3 to 11 and was adjusted by 0.01M HCl acid or 0.01M NaOH. The adsorbent dose and kinetic reaction were varied from 0.05 to 0.4 g L^{-1} and from 5 to 120 min, respectively. The separation of the solid-liquid phases was performed by centrifuging. The residual concentration was determined using a UV/Vis spectrophotometer (2300/Techcomp) at 376 nm as λ_{max} of TC. The quantity adsorbed q_e (mg g^{-1}) and the and TC removal efficiency (%) were obtained using the following formulas (El Messaoudi et al., 2016b):

$$q_e = \frac{(C_0 - C_e) \times V}{w} \quad (1)$$

$$\% \, Removal = \frac{(C_0 - C_e)}{C_0} \times 100 \quad (2)$$

In Eqs. (1) and (2), C_0 (mg L^{-1}) and C_e (mg L^{-1}) denote the concentrations of TC before and after adsorption, respectively. The w (g) and V (L) represents the weight of SiO_2 NPs and the volume of the reaction solution, respectively.

2.5 Design of experiment runs

BBD used a static method for the design of experimental parameters influencing the adsorption of TC on SiO_2 NPs using design-expert software (version 12.0.3). TC concentration (A), reaction time (B), and SiO_2 NPs dose (C) as factors have significant effects on the TC adsorption on SiO_2 NPs at 23±1°C and pH=5. Design of experiment runs and corresponding responses for TC removal efficiency by SiO_2 NPs are summarized in **Table 1**. A three-factors and levels (–1, 0, and 1) were applied to 21 experiments. The TC removal efficiency R (%) was expressed using the quadratic polynomial model was formalized in Eq.3 (Jawad et al., 2020):

$$R(\%) = \sum_{I=1}^{3} \delta_i X_i + \sum_{I=1}^{3} \delta_{ii} {X_i}^2 + \sum_{I<j} \delta_{ij} X_i X_j + \delta_0 \quad (3)$$

In Eq.3, δ_0 denotes constant-coefficient, δ_i is attributed to the direct effect, δ_{ii} corresponds to higher-order effect, and δ_{ij} denote reciprocate effect.

3 Results and discussion

3.1 SiO_2 NPs characterization

The microstructures of synthesized nanoparticles were analyzed using SEM coupled with EDX. The results obtained are shown in **Fig.1**. According to **Fig. 1a**, The SEM image of SiO_2 NPs showed that the particles are agglomerated and have poor dispersion. **Fig.1b** represents the EDX spectrum and elemental analysis of SiO_2 NPs. The synthesis of SiO_2 NPs confirmed by the presence of O (53.82 %) and Si (46.18 %) (Dubey et al., 2015). **Fig 1c** and **d** indicate the uniform distribution of O and Si was illustrated by EDX elemental mapping.

Fig.2 illustrates the N_2 isotherms adsorption-desorption and average diameter distribution for SiO_2 NPs nanospheres. By means, BET and BJH methods, the obtained average surface area, pore diameter, and total pore volume were 583.46 $m^2\ g^{-1}$, 3.46 nm, and 0.27 $cm^3\ g^{-1}$, respectively, confirmed the porosity of SiO_2 NPs.

The FT-IR spectra results are depicted in **Fig.3**. The broad bands at 3452 cm^{-1} and 1634 cm^{-1} correspond to OH stretching vibration and absorbed water molecule, respectively (El Messaoudi et al., 2016a; Niksefat et al., 2014). The peaks at 1083 cm^{-1}, 953 cm^{-1} and 806 cm^{-1} and 457 cm^{-1} were ascribed to the Si-O stretching vibration, Si-OH stretching vibration and Si-O-Si symmetric stretching, and Si-O-Si bending, respectively (Rafigh and Heydarinasab, 2017; Yue et al., 2019), which confirms successful synthesis of SiO_2 nanospheres. The spectrum of TC-SiO_2 NPs shows small changes that demonstrate the TC adsorption on the surface of SiO_2 NPs.

Fig.4a shows the nanoparticles of SiO_2 NPs using a TEM image. According to this figure, the synthesized SiO_2 NPs particles were found to be spherical in structure. The XRD characterization results of SiO_2 NPs are provided in **Fig.4b**. A broad peak in the range of 20–30° is corresponded to SiO_2 (Rafigh and Heydarinasab, 2017), indicating the successful synthesis of SiO_2 NPs.

3.2 TC adsorption study

3.2.1 Solution pH

Fig. 5a presents the influence of pH on the TC adsorption at pH values ranging from 3 to11. In this experiment, 10 mg of SiO_2 NPs were attempted in 50 mL of the solution TC (50 mg L^{-1}) at T=23 ±1°C for 120 min. As **Fig. 5a** shows, the highest removal of TC was 98.07 % at pH 5. Debnath et al. (2020) and Rashidi Nodeh et al. (2020) obtained even results. This increase of TC removal in the acidic medium can be explained by the charge positive of SiO_2 NPs and the charge negative of TC.

3.2.2 SiO_2 NPs dose

A TC concentration of 50 mg L^{-1} with a pH 5 at T=23 ± 1 for 120 min, the effect of SiO_2 NPs dose (0.05-0.4 g L^{-1}) on TC adsorption was studied. **Fig.5b** shows the results obtained. The TC removal increased from 54.38 to 98.92 % by increasing the SiO_2 NPs amount from 0.05 to 0.25 g L^{-1}, while the quantity adsorbed decreased from 543.88 to 197.95 mg g^{-1}. Results imply that the number of active adsorption sites for TC adsorption corresponds to the applied dose, prompting higher removal efficiency (Jin et al., 2019). After equilibrium between the adsorbent and antibiotic solution, the removal percentage remains consistent at higher dosages (>0.25 g L^{-1}). The optimum adsorbent dosage was considered 0.25 g L^{-1} to reach maximum TC removal efficiency, respectively.

3.2.3 Contact time

The influence of the contact time on TC adsorption using SiO_2 NPs displayed in **Fig.5a**. The contact time ranged from 5 to 120 minutes, whereas other parameters were kept constant (SiO_2 NPs=0.25 g L^{-1}, TC concentration=50 mg L^{-1}, pH=5, and T=23±1°C). The TC adsorption was fast at first 40 min. This may be attributed to many sites that are accessible on the surface of the SiO_2 NPs in the initial phase. With decreasing in several active sites, the adsorption rate became consistent (Zhou et al., 2020). Experimental data showed that stability was achieved in 40 min with an adsorption capacity of TC was 195.97 mg g^{-1}.

3.2.4 TC concentration

The influence of TC concentration (25–200 mg L^{-1}) on its retention using SiO_2 NPs was studied with a fixed pH 5 and 0.25 g L^{-1} of SiO_2 NPs dose for 40 min. As illustrated in **Fig.5d**, by increasing TC concentration, the TC adsorption capacity progressively increased owing to the occupation of all available sites on the surface of nanoparticles by TC molecules. But, a plateau was not achieved in the adsorption capacity, suggesting active sites are still available and no saturation occurred (Ravikumar et al., 2019).

3.2.5 Effect of Ionic Strength

The electrolyte (NaCl) concentration in the aqueous solution affects significantly TC adsorption onto SiO_2 NPs. As reported in **Fig. 6**, at SiO_2 NPs=0.25 g L^{-1}, TC concentration=50 mg L^{-1}, pH=7, and T=23±1°C, the removal efficiency of SiO_2 NPs for TC decreased from 73.15 % (0 M NaCl) to 55.48 % (0.4 M NaCl) by increasing the electrolyte concentrations from 0 to 0.4 M NaCl. By increasing the ionic strength, Cl^- competes with negatively charged TC (TCH^-, TC^-) species for adsorption sites onto SiO_2 NPs surface site with positively charged at pH 7. This result is in line with another study that reported a decline in TC adsorption onto clay surface sites with negatively charged by increasing

electrolyte concentration in the solution (Parolo et al., 2008). In their study, by increasing Na^+ ion concentration at pH 4 of the solution, the competence for occupying surface sites between Na^+ ion and positively charged TC (TCH^+) increased. The reduction in TC adsorption onto the surface of clay increased in a higher concentration of Na^+ (Parolo et al., 2008).

3.3 Adsorption kinetics

The obtained experimental data were evaluated by using the pseudo 1st order (PFO), pseudo 2nd order (PSO), and intraparticle diffusion (IPD) kinetic models, and their linear forms are given using the following Eqs. (4), (5), and (6) as represented in **Table 2** (Bentahar et al., 2018; El Messaoudi et al., 2017). **Table 2** shows the parameters for linear fitting. As represented in **Table 2**, the PSO model was fitted to data experimental based on R^2 (correlation coefficient). It can be found that R^2 values are very near to 1, and the $q_{e,exp}$ values are also closer to $q_{e,cal}$ values for the PSO. In this model, it is speculated that adsorption pursues a second-order mechanism (Bao et al., 2018; El Messaoudi et al., 2021).

3.4 Adsorption isotherm

The TC adsorption on SiO_2 NPs was the Langmuir, Freundlich, and Temkin isotherm models. The linear forms of these isotherms are expressed on Eqs. (7), (8), and (9) as represented in **Table 3** (Xu et al., 2019). The parameters of linear fitting are listed in **Table 3**. Based on regression coefficients R^2, the Langmuir isotherm describes the adsorption in the monolayer process (Ani et al., 2020). The *Qm* of SiO_2 NPs for TC adsorption was 552.48 mg g^{-1}. **Table 4** show that SiO_2 NPs exhibit high adsorption of TC compared with adsorbents. This result indicates that the SiO_2 NPs is a suitable adsorbent for wastewater treatment.

3.5 Design optimization

Table 5 presents the results of ANOVA analysis of the statistical significance. The p-value (<0.0001) indicates the polynomial equation was significant for the removal of TC on SiO_2 NPs within 95 % (Hu et al., 2021). The high values of R^2 (0.9925), adjusted R^2 (0.9864), and

predicted R^2 (0.9449) indicated the excellent fit of this model to the factors selected. The value of adequate precision of 37.9356 (>4) shows a high level of statistical significance (Oyekanmi et al., 2019). The predicated TC removal using SiO_2 NPs was obtained by the developed model represented below in Eq. (10):

$$R\ (\%) = 98.57 - 6.84\,A + 3.78\,B + 0.8861\,C + 3.72\,AB + 0.6362\,AC - 0.0713\,BC - 3.57A^2 - 2.36\,B^2 - 0.6527\,C^2 \quad (10)$$

The residual *vs.* predicted and 3D response surface plots of TC percentage are illustrated in **Fig.7** and **Fig.8**, respectively. The TC removal was experimentally 99.56 % under optimal conditions (SiO_2 NPs dose=0.25 g L^{-1}, C_0=25 mg L^{-1}, and pH=5 at 23±1°C for 40 min) RSM-BBD modeling.

3.6 Adsorption mechanism

The adsorption mechanism of TC on SiO_2 NPs is schematized in **Fig.9 b** based on PZC. As **Fig.9a** shows, PZC of SiO_2 NPs was 8.2. The dominance of charge positive of SiO_2 NPs at pH<PZC and negatively charged when pH>PZC. The high value of PZC indicates the favorable and maximum adsorption in an acidic medium. This result confirmed the effect of pH on adsorption. The charge positive of SiO_2 NPs and the negative charge of TC indicates the governance of electrostatic interactions between TC and SiO_2 NPs.

3.7 Reusability of SiO_2 NPs

To assess the applicability of the adsorbent in the full-scale operation, the reusable capacity of SiO_2 NPs was studied for the removal of TC in optimal conditions (SiO_2 NPs dose=0.25 g L^{-1}, t=40 min, C_0=50 mg L^{-1}, pH (TC)=5, and T=23±1°C). Therefore, the regeneration studies for evaluating the adsorption efficiency of the nanocomposite were conducted within five successive cycles using 0.1 M NaOH. According to **Fig.10**, less than a 13 % drop in the removal efficiency of TC occurred at the end of the fifth run, signifying the desirable reusability potential of the synthesized nanoparticles within successive runs of operation. In

conclusion, the present adsorbent can be regarded as a promising material for practical application in environmental protection purposes due to its excellent adsorption activities and high stability.

4 Conclusions

The SiO_2 nanoparticles biosynthesized from the extract *Nerium oleander* leaves are effective in removing tetracycline (TC) from an aqueous solution. The result of SEM-EDX, FTIR, TEM, and XRD characterization confirmed the biosynthesis of SiO_2 NPs successfully. Under conditions (SiO_2 NPs dose=0.25 g L^{-1}, t=40 min, C_0=50 mg L^{-1}, pH (TC)=5, and T=23±1°C), the TC removal was 98.62 %. The TC adsorption on SiO_2 NPs followed the PSO and Langmuir models. The Qm was 552.48 mg g^{-1}. The recyclability study demonstrated that the SiO_2 NPs exhibited excellent reusability for TC removal. Optimization is an effective approach for modeling the sorption process of the TC on SiO_2 NPs using BBD–RSM. These results confirm that the SiO_2 NPs nanoparticles are suitable for removing antibiotics from wastewaters.

References

Aalipour, F., Mirlohi, M., Jalali, M., 2014. Determination of antibiotic consumption index for animal originated foods produced in animal husbandry in Iran, 2010. J. Environ. Heal. Sci. Eng. 2014 121 12, 1–7. https://doi.org/10.1186/2052-336X-12-42

Ahamad, T., Ruksana, Chaudhary, A.A., Naushad, M., Alshehri, S.M., 2019. Fabrication of MnFe2O4 nanoparticles embedded chitosan-diphenylureaformaldehyde resin for the removal of tetracycline from aqueous solution. Int. J. Biol. Macromol. 134, 180–188. https://doi.org/10.1016/J.IJBIOMAC.2019.04.204

Ani, J.U., Akpomie, K.G., Okoro, U.C., Aneke, L.E., Onukwuli, O.D., Ujam, O.T., 2020. Potentials of activated carbon produced from biomass materials for sequestration of dyes, heavy metals, and crude oil components from aqueous environment. Appl. Water Sci. 2020 102 10, 1–11. https://doi.org/10.1007/S13201-020-1149-8

Bao, J., Zhu, Y., Yuan, S., Wang, F., Tang, H., Bao, Z., Zhou, H., Chen, Y., 2018. Adsorption of Tetracycline with Reduced Graphene Oxide Decorated with MnFe 2 O 4 Nanoparticles. Nanoscale Res. Lett. 2018 131 13, 1–8. https://doi.org/10.1186/S11671-018-2814-9

Bentahar, S., Dbik, A., Khomri, M.E., El Messaoudi, N., Lacherai, A., 2018. Removal of a cationic dye from aqueous solution by natural clay. Groundw. Sustain. Dev. 6, 255–262. https://doi.org/10.1016/j.gsd.2018.02.002

Chen, K.-H., Pu, Y.-C., Chang, K.-D., Liang, Y.-F., Liu, C.-M., Yeh, J.-W., Shih, H.-C., Hsu, Y.-J., 2012. Ag-Nanoparticle-Decorated SiO2 Nanospheres Exhibiting Remarkable Plasmon-Mediated Photocatalytic Properties. J. Phys. Chem. C 116, 19039–19045. https://doi.org/10.1021/JP306555J

Daghrir, R., Drogui, P., 2013. Tetracycline antibiotics in the environment: a review. Environ. Chem. Lett. 2013 113 11, 209–227. https://doi.org/10.1007/S10311-013-0404-8

293 Das, R., Vecitis, C.D., Schulze, A., Cao, B., Ismail, A.F., Lu, X., Chen, J., Ramakrishna, S.,
294 2017. Recent advances in nanomaterials for water protection and monitoring. Chem. Soc.
295 Rev. 46, 6946–7020. https://doi.org/10.1039/C6CS00921B
296 Das, S., Chakraborty, J., Chatterjee, S., Kumar, H., 2018. Prospects of biosynthesized
297 nanomaterials for the remediation of organic and inorganic environmental contaminants.
298 Environ. Sci. Nano 5, 2784–2808. https://doi.org/10.1039/C8EN00799C
299 Debnath, B., Majumdar, M., Bhowmik, M., Bhowmik, K.L., Debnath, A., Roy, D.N., 2020.
300 The effective adsorption of tetracycline onto zirconia nanoparticles synthesized by novel
301 microbial green technology. J. Environ. Manage. 261, 110235.
302 https://doi.org/10.1016/j.jenvman.2020.110235
303 Dubey, R.S., Rajesh, Y.B.R.D., More, M.A., 2015. Synthesis and Characterization of SiO2
304 Nanoparticles via Sol-gel Method for Industrial Applications. Mater. Today Proc. 2,
305 3575–3579. https://doi.org/10.1016/J.MATPR.2015.07.098
306 El Khomri, M., El Messaoudi, N., Dbik, A., Bentahar, S., Lacherai, A., 2020. Efficient
307 adsorbent derived from Argania Spinosa for the adsorption of cationic dye: Kinetics,
308 mechanism, isotherm and thermodynamic study. Surfaces and Interfaces 20, 100601.
309 https://doi.org/10.1016/j.surfin.2020.100601
310 El Messaoudi, N., Dbik, A., El Khomri, M., Sabour, A., Bentahar, S., Lacherai, A., 2017.
311 Date stones of Phoenix dactylifera and jujube shells of Ziziphus lotus as potential
312 biosorbents for anionic dye removal. Int. J. Phytoremediation 19, 1047–1052.
313 https://doi.org/10.1080/15226514.2017.1319331
314 El Messaoudi, N., El Khomri, M., Bentahar, S., Dbik, A., Lacherai, A., Bakiz, B., 2016a.
315 Evaluation of performance of chemically treated date stones: Application for the removal
316 of cationic dyes from aqueous solutions. J. Taiwan Inst. Chem. Eng. 67, 244–253.
317 https://doi.org/10.1016/j.jtice.2016.07.024
318 El Messaoudi, N., El Khomri, M., Dabagh, A., Chegini, Z.G., Dbik, A., Bentahar, S.,

Lacherai, A., Iqbal, M., Jada, A., Sher, F., Lima, É.C., 2021. Synthesis of a novel nanocomposite based on date stones/CuFe $_2$ O $_4$ nanoparticles for eliminating cationic and anionic dyes from aqueous solution. Int. J. Environ. Stud. 1–19. https://doi.org/10.1080/00207233.2021.1929469

El Messaoudi, N., El Khomri, M., Dbik, A., Bentahar, S., Lacherai, A., Bakiz, B., 2016b. Biosorption of Congo red in a fixed-bed column from aqueous solution using jujube shell: Experimental and mathematical modeling. J. Environ. Chem. Eng. 4, 3848–3855. https://doi.org/10.1016/j.jece.2016.08.027

Epps, A. Van, Blaney, L., 2016. Antibiotic Residues in Animal Waste: Occurrence and Degradation in Conventional Agricultural Waste Management Practices. Curr. Pollut. Reports 2016 23 2, 135–155. https://doi.org/10.1007/S40726-016-0037-1

Fiol, N., Villaescusa, I., 2009. Determination of sorbent point zero charge: Usefulness in sorption studies. Environ. Chem. Lett. 7, 79–84. https://doi.org/10.1007/s10311-008-0139-0

Grenni, P., Ancona, V., Barra Caracciolo, A., 2018. Ecological effects of antibiotics on natural ecosystems: A review. Microchem. J. 136, 25–39. https://doi.org/10.1016/J.MICROC.2017.02.006

Hosseini, S.A., Vossoughi, M., Mahmoodi, N.M., Sadrzadeh, M., 2018. Efficient dye removal from aqueous solution by high-performance electrospun nanofibrous membranes through incorporation of SiO2 nanoparticles. J. Clean. Prod. 183, 1197–1206. https://doi.org/10.1016/j.jclepro.2018.02.168

Hu, Y. ying, Pan, C., Zheng, X., Hu, F., Xu, L., Xu, G., Jian, Y., Peng, X., 2021. Prediction and optimization of adsorption properties for Cs+on NiSiO@NiAlFe LDHs hollow spheres from aqueous solution: Kinetics, isotherms, and BBD model. J. Hazard. Mater. 401, 123374. https://doi.org/10.1016/J.JHAZMAT.2020.123374

Ibrahim, R.K., Hayyan, M., AlSaadi, M.A., Hayyan, A., Ibrahim, S., 2016. Environmental

345 application of nanotechnology: air, soil, and water. Environ. Sci. Pollut. Res. 2016 2314
346 23, 13754–13788. https://doi.org/10.1007/S11356-016-6457-Z
347 Jawad, A.H., Malek, N.N.A., Abdulhameed, A.S., Razuan, R., 2020. Synthesis of Magnetic
348 Chitosan-Fly Ash/Fe3O4 Composite for Adsorption of Reactive Orange 16 Dye:
349 Optimization by Box–Behnken Design. J. Polym. Environ. 28, 1068–1082.
350 https://doi.org/10.1007/s10924-020-01669-z
351 Jin, J., Yang, Z., Xiong, W., Zhou, Y., Xu, R., Zhang, Y., Cao, J., Li, X., Zhou, C., 2019. Cu
352 and Co nanoparticles co-doped MIL-101 as a novel adsorbent for efficient removal of
353 tetracycline from aqueous solutions. Sci. Total Environ. 650, 408–418.
354 https://doi.org/10.1016/J.SCITOTENV.2018.08.434
355 Li, S., Huang, W., Yang, P., Li, Z., Xia, B., Li, M., Xue, C., Liu, D., 2021. One-pot synthesis
356 of N-doped carbon intercalated molybdenum disulfide nanohybrid for enhanced
357 adsorption of tetracycline from aqueous solutions. Sci. Total Environ. 754, 141925.
358 https://doi.org/10.1016/J.SCITOTENV.2020.141925
359 Liu, F., Zhang, W., Chen, W., Wang, Jing, Yang, Q., Zhu, W., Wang, Jianlong, 2017. One-pot
360 synthesis of NiFe2O4 integrated with EDTA-derived carbon dots for enhanced removal
361 of tetracycline. Chem. Eng. J. 310, 187–196. https://doi.org/10.1016/J.CEJ.2016.10.116
362 Martín, A., Caldelas, C., Weiss, D., Aranjuelo, I., Navarro, E., 2018. Assessment of Metal
363 Immission in Urban Environments Using Elemental Concentrations and Zinc Isotope
364 Signatures in Leaves of Nerium oleander. Environ. Sci. Technol. 52, 2071–2080.
365 https://doi.org/10.1021/ACS.EST.7B00617
366 Niksefat, N., Jahanshahi, M., Rahimpour, A., 2014. The effect of SiO2 nanoparticles on
367 morphology and performance of thin film composite membranes for forward osmosis
368 application. Desalination 343, 140–146. https://doi.org/10.1016/J.DESAL.2014.03.031
369 Oyekanmi, A.A., Ahmad, A., Hossain, K., Rafatullah, M., 2019. Statistical optimization for
370 adsorption of Rhodamine B dye from aqueous solutions. J. Mol. Liq. 281, 48–58.

371 https://doi.org/10.1016/J.MOLLIQ.2019.02.057
372 Parolo, M.E., Savini, M.C., Vallés, J.M., Baschini, M.T., Avena, M.J., 2008. Tetracycline
373 adsorption on montmorillonite: pH and ionic strength effects. Appl. Clay Sci. 40, 179–
374 186. https://doi.org/10.1016/J.CLAY.2007.08.003
375 Rafigh, S.M., Heydarinasab, A., 2017. Mesoporous Chitosan–SiO2 Nanoparticles: Synthesis,
376 Characterization, and CO2 Adsorption Capacity. ACS Sustain. Chem. Eng. 5, 10379–
377 10386. https://doi.org/10.1021/ACSSUSCHEMENG.7B02388
378 Rashidi Nodeh, H., Sereshti, H., Beirakabadi, E., Razmkhah, K., 2020. Synthesis and
379 application of lanthanum sulfide nanoparticles for removal of tetracycline from aqueous
380 media. Int. J. Environ. Sci. Technol. 17, 819–828. https://doi.org/10.1007/s13762-019-
381 02399-z
382 Ravikumar, K.V.G., Sudakaran, S.V., Ravichandran, K., Pulimi, M., Natarajan, C.,
383 Mukherjee, A., 2019. Green synthesis of NiFe nano particles using Punica granatum peel
384 extract for tetracycline removal. J. Clean. Prod. 210, 767–776.
385 https://doi.org/10.1016/j.jclepro.2018.11.108
386 Rostam, A.B., Taghizadeh, M., 2020. Advanced oxidation processes integrated by membrane
387 reactors and bioreactors for various wastewater treatments: A critical review. J. Environ.
388 Chem. Eng. 8, 104566. https://doi.org/10.1016/J.JECE.2020.104566
389 Scaria, J., Anupama, K. V., Nidheesh, P. V., 2021. Tetracyclines in the environment: An
390 overview on the occurrence, fate, toxicity, detection, removal methods, and sludge
391 management. Sci. Total Environ. 771, 145291.
392 https://doi.org/10.1016/J.SCITOTENV.2021.145291
393 Sebeia, N., Jabli, M., Ghith, A., 2019. Biological synthesis of copper nanoparticles, using
394 Nerium oleander leaves extract: Characterization and study of their interaction with
395 organic dyes. Inorg. Chem. Commun. 105, 36–46.
396 https://doi.org/10.1016/J.INOCHE.2019.04.023

Sharma, G., Bhogal, S., Kumar, A., Naushad, M., Sharma, S., Ahamad, T., Stadler, F.J., 2020. AgO/MgO/FeO@Si3N4 nanocomposite with robust adsorption capacity for tetracycline antibiotic removal from aqueous system. Adv. Powder Technol. 31, 4310–4318. https://doi.org/10.1016/J.APT.2020.09.006

Sharma, P., Kherb, J., Prakash, J., Kaushal, R., 2021. A novel and facile green synthesis of SiO2 nanoparticles for removal of toxic water pollutants. Appl. Nanosci. 2021 1–13. https://doi.org/10.1007/S13204-021-01898-1

Sodhi, K.K., Kumar, M., Balan, B., Dhaulaniya, A.S., Shree, P., Sharma, N., Singh, D.K., 2021. Perspectives on the antibiotic contamination, resistance, metabolomics, and systemic remediation. SN Appl. Sci. 2021 32 3, 1–25. https://doi.org/10.1007/S42452-020-04003-3

Song, Y.X., Chen, S., You, N., Fan, H.T., Sun, L.N., 2020. Nanocomposites of zero-valent Iron@Activated carbon derived from corn stalk for adsorptive removal of tetracycline antibiotics. Chemosphere 255, 126917. https://doi.org/10.1016/J.CHEMOSPHERE.2020.126917

Suba, V., Rathika, G., Kumar, E.R., Saravanabhavan, M., 2018. Influence of Magnetic Nanoparticles on Surface Changes in CoFe 2 O 4 /Nerium Oleander Leaf Waste Activated Carbon Nanocomposite for Water Treatment. J. Inorg. Organomet. Polym. Mater. 2018 285 28, 1706–1717. https://doi.org/10.1007/S10904-018-0831-X

Van, T.T.H., Yidana, Z., Smooker, P.M., Coloe, P.J., 2020. Antibiotic use in food animals worldwide, with a focus on Africa: Pluses and minuses. J. Glob. Antimicrob. Resist. 20, 170–177. https://doi.org/10.1016/J.JGAR.2019.07.031

Wang, X., Li, F., Hu, X., Hua, T., 2021. Electrochemical advanced oxidation processes coupled with membrane filtration for degrading antibiotic residues: A review on its potential applications, advances, and challenges. Sci. Total Environ. 784, 146912. https://doi.org/10.1016/J.SCITOTENV.2021.146912

Xu, G., Zhu, Y., Wang, X., Wang, S., Cheng, T., Ping, R., Cao, J., Lv, K., 2019. Novel chitosan and Laponite based nanocomposite for fast removal of Cd(II), methylene blue and Congo red from aqueous solution. e-Polymers 19, 244–256. https://doi.org/10.1515/EPOLY-2019-0025

Yu, F., Li, Y., Han, S., Ma, J., 2016. Adsorptive removal of antibiotics from aqueous solution using carbon materials. Chemosphere 153, 365–385. https://doi.org/10.1016/J.CHEMOSPHERE.2016.03.083

Yue, Y., Peng, Z., Wang, W., Cai, Y., Tan, F., Wang, X., Qiao, X., 2019. Facile preparation of MgO-loaded SiO2 nanocomposites for tetracycline removal from aqueous solution. Powder Technol. 347, 1–9. https://doi.org/10.1016/J.POWTEC.2019.02.034

Zhou, J., Ma, F., Guo, H., 2020. Adsorption behavior of tetracycline from aqueous solution on ferroferric oxide nanoparticles assisted powdered activated carbon. Chem. Eng. J. 384, 123290. https://doi.org/10.1016/J.CEJ.2019.123290

448 # List of Figures

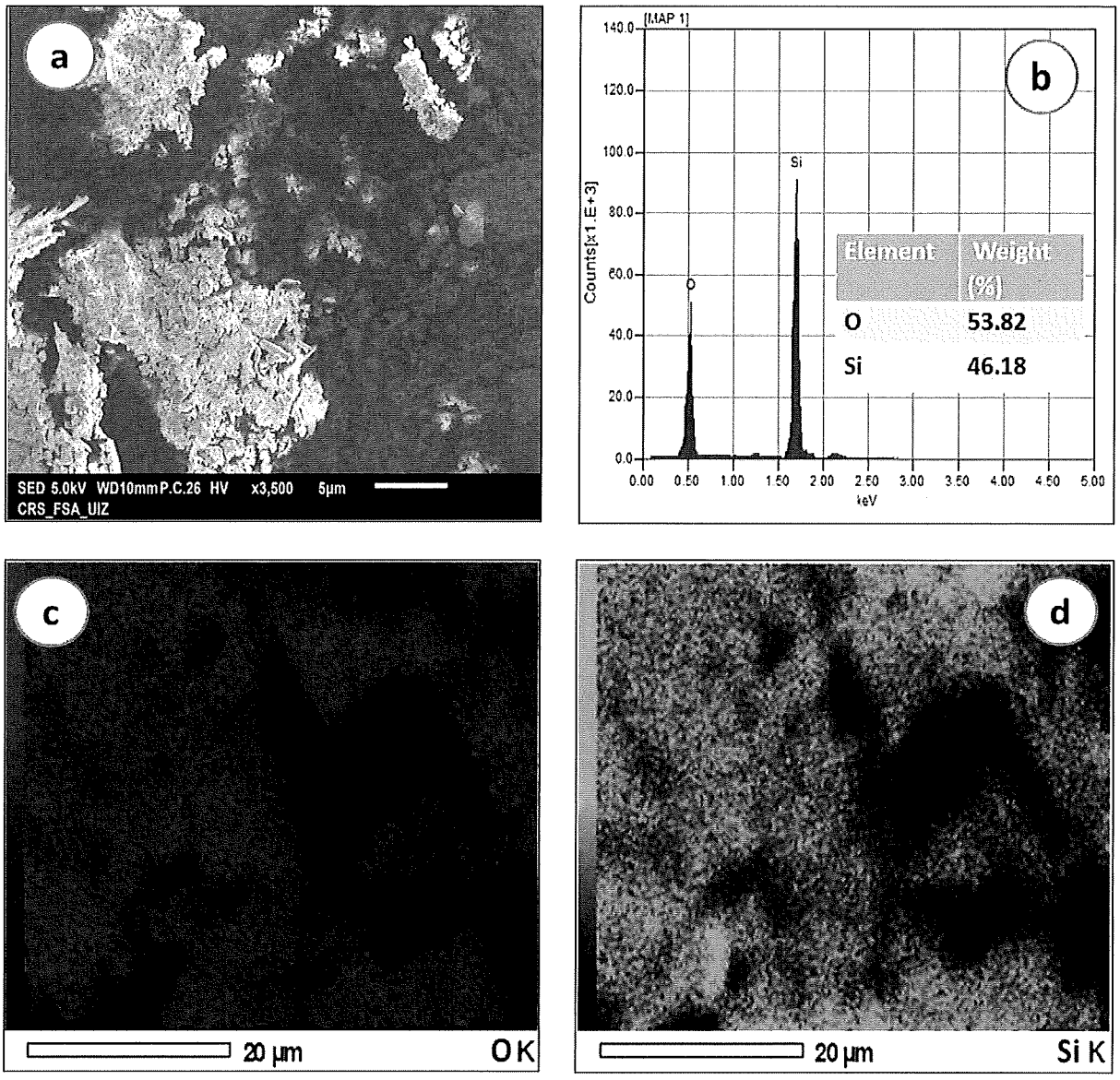

449 **Fig.1**.SEM image (**a**), elemental analysis (**b**) and mapping images of SiO_2 NPs: oxygen (**c**)

450 and silicon (**d**).

451

452

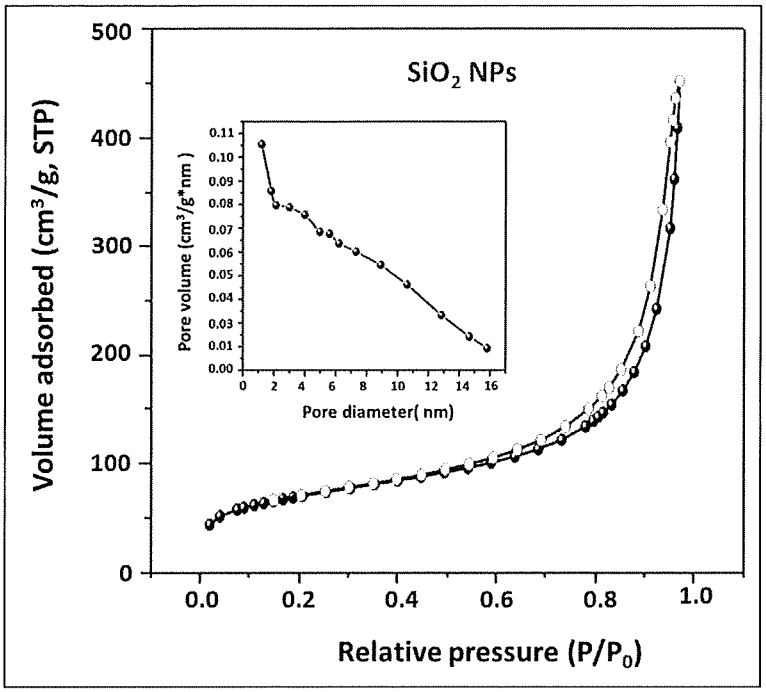

453

454 **Fig.2**. N_2 adsoption/desorption isotherms included pore size distributions curves

455 of TC-SiO_2 NPs.

456

457

458

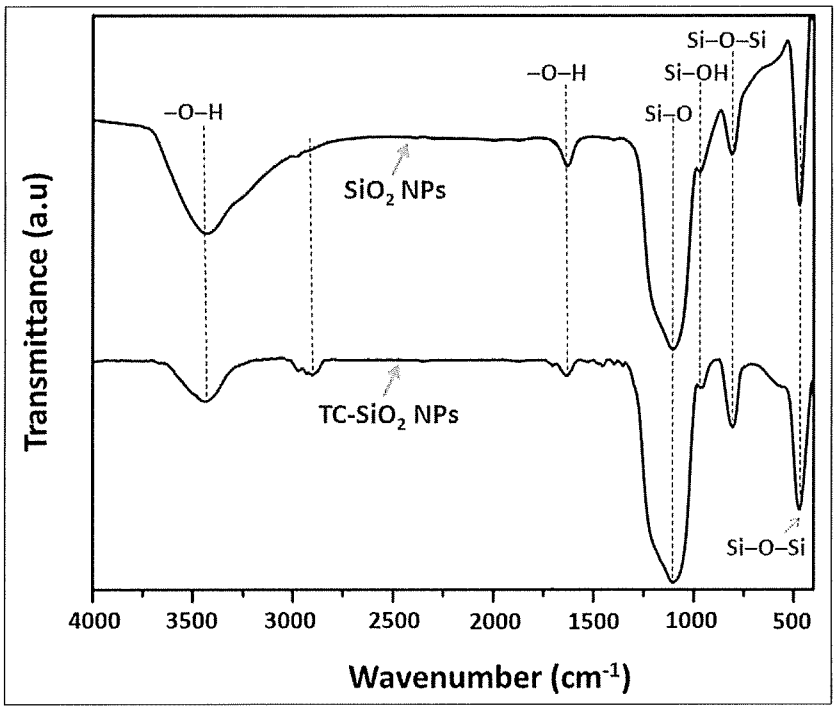

459 **Fig.3**. FTIR spectra of SiO_2 NPs and TC-SiO_2 NPs.

460

461

462

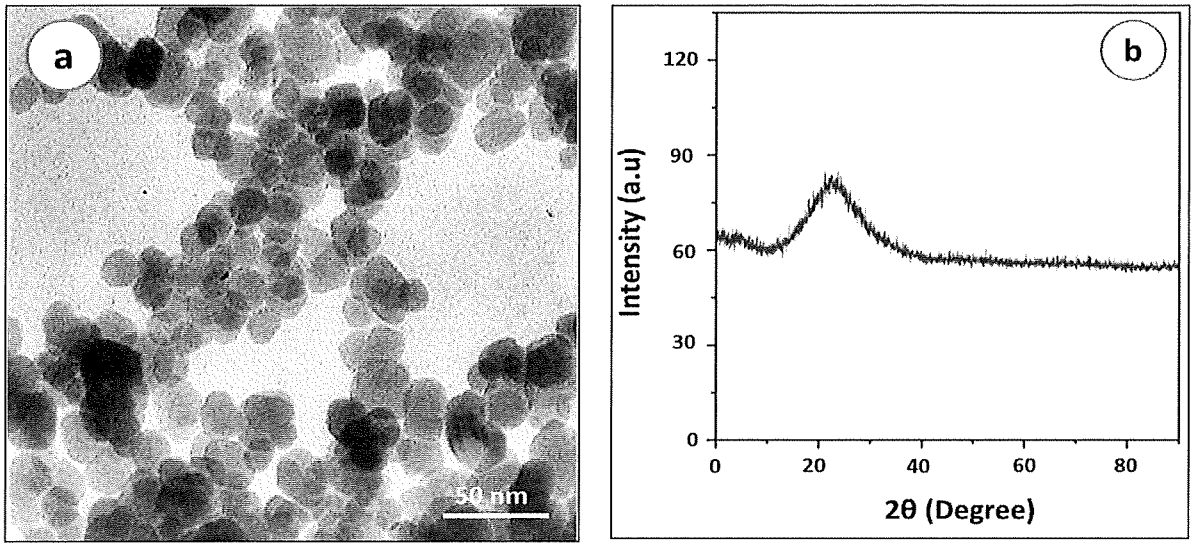

463 **Fig.4**. TEM image (**a**) and XRD pattern (**b**) of SiO_2 NPs.

464

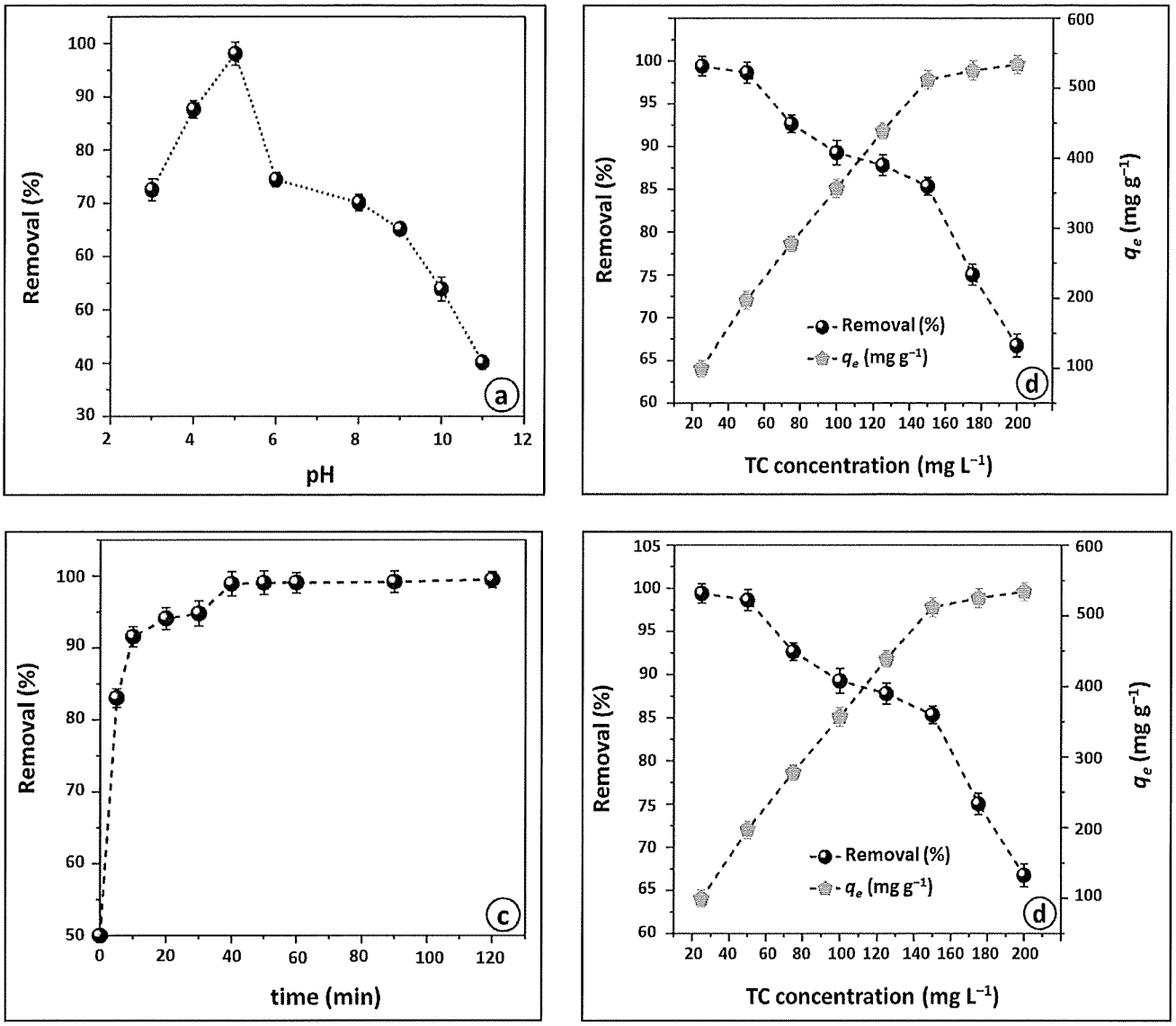

465 **Fig.5**. Effects of pH (**a**), SiO_2 NPs dose (**b**), reaction time (**c**), and TC concentration

466 (**d**) on TC adsorption using SiO_2 NPs.

467

468

469

470

471

472

473

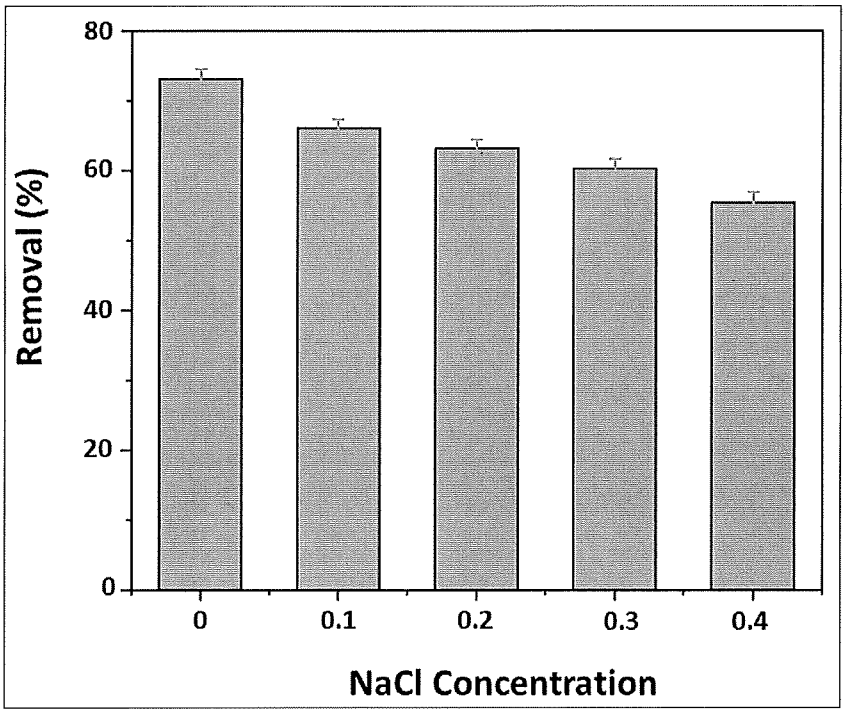

474

475 **Fig.6**. The effect of ionic strength on TC adsorption using SiO_2 NPs.

476

477

478

479

480

481

482

483

484

485

486

487

488

489

490

491

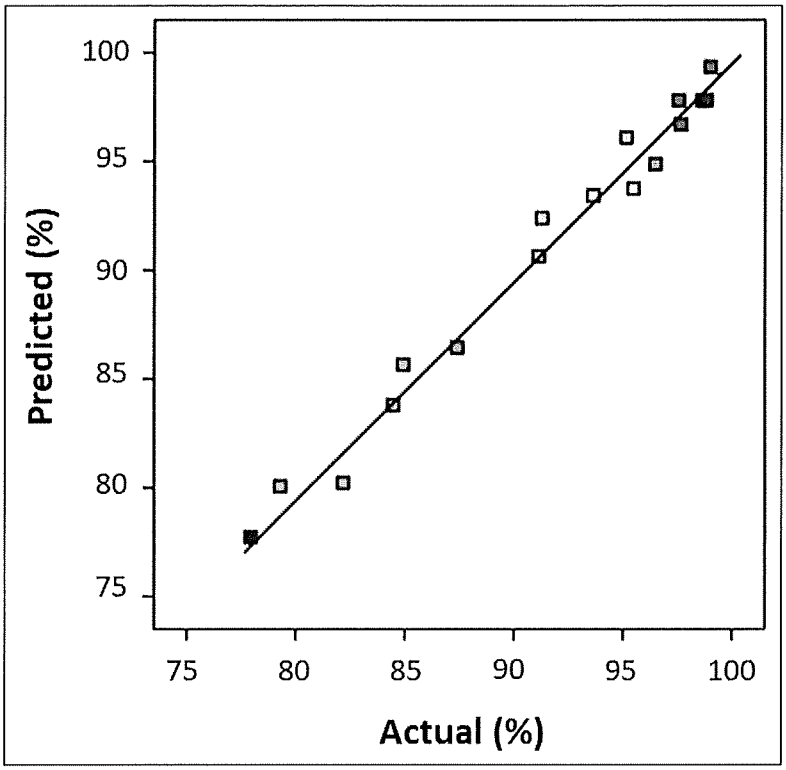

492

493 **Fig.7**. Actual versus predicted for TC adsorption on SiO_2 NPs.

494

495

496

497

498

499

500

501

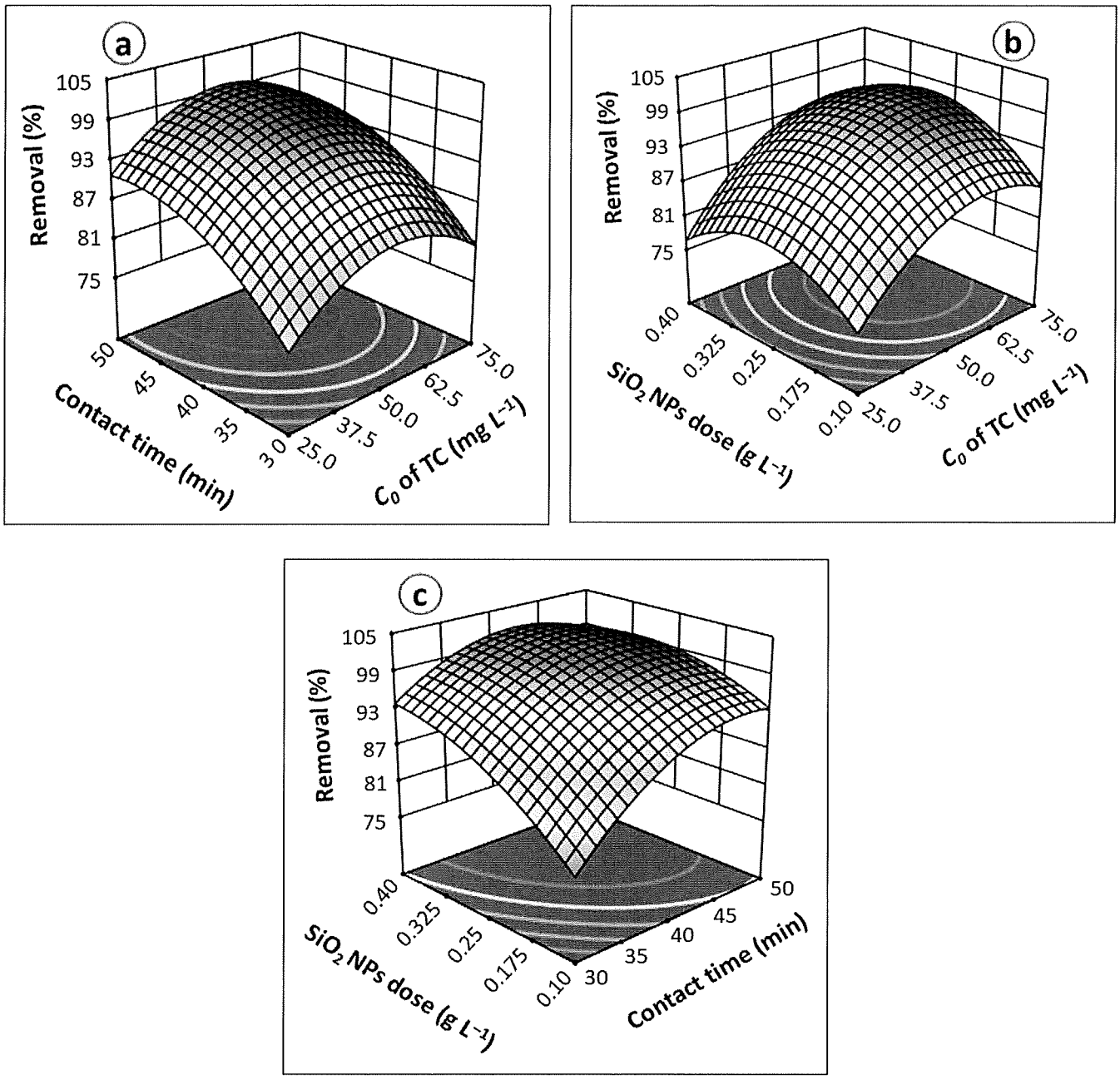

502 **Fig.8**. Surface response plots of TC removal percentage: initial TC concentration with contact
503 time (**a**), SiO_2 NPs dose with initial TC concentration (**b**), SiO_2 NPs dose, and with contact
504 time (**c**).

505

506

507

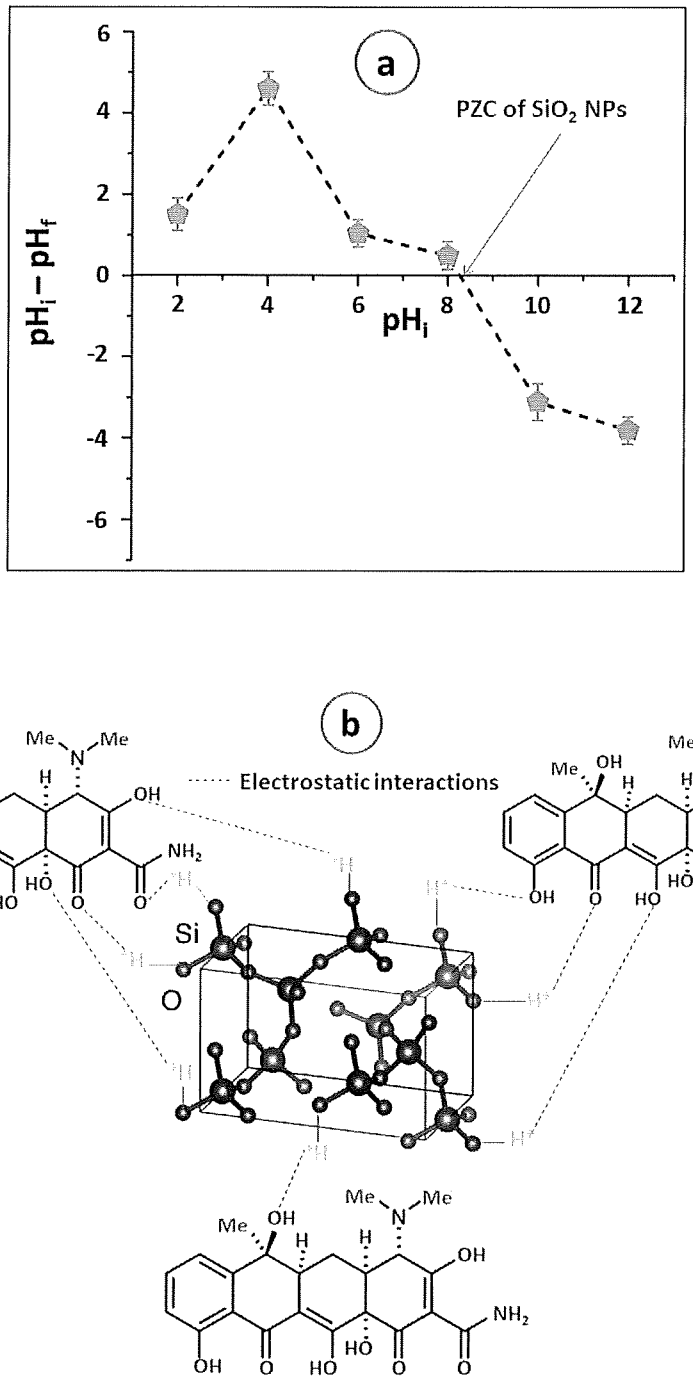

508 **Fig.9**. PZC of SiO_2 NPs (**a**) and proposed adsorption mechanism of TC on SiO_2 NPs (**b**).

509

510

511

512

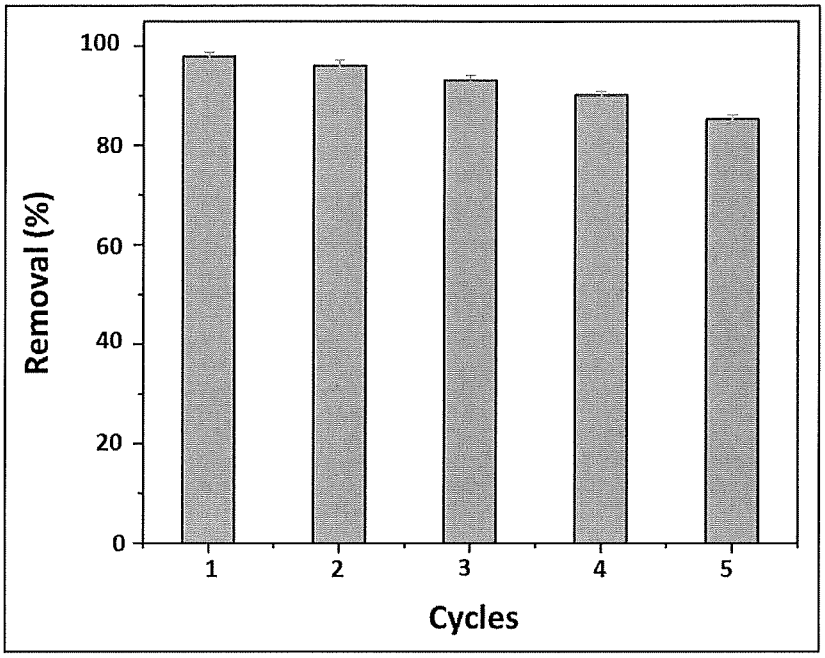

Fig.10. Reusability of SiO_2 NPs for the removal of TC.

524 # List of Tables

525 **Table 1**. Design of experiment runs and correspondents responses for TC removal efficiency

526 by SiO_2 NPs.

Variables			**Codes**		
			-1	0	1
A=TC concentration (mg L^{-1})			25	50	75
B=Contact time (min)			30	40	50
C=SiO_2 NPs dose (g L^{-1})			0.1	0.25	0.4
Run	**A**	**B**	**C**		**R**
	(mg L^{-1})	(min)	**(g L^{-1})**		**(%)**
1	25	30	0.1		98.05
2	75	30	0.1		77.11
3	25	50	0.1		98.87
4	75	50	0.1		90.11
5	25	30	0.4		99.23
6	75	30	0.4		78.13
7	25	50	0.4		99.06
8	75	50	0.4		93.55
9	25	40	0.25		99.56
10	75	40	0.25		90.57
11	50	30	0.25		89.45
12	50	50	0.25		98.66
13	50	40	0.1		90.11
14	50	40	0.4		98.65
15	50	40	0.25		98.44
16	50	40	0.25		98.71
17	50	40	0.25		98.24
18	50	40	0.25		98.53
19	50	40	0.25		98.61
20	50	40	0.25		98.72
21	50	40	0.25		98.23

527

528 **Table 2.** TC adsorption kinetic parameters using SiO_2 NPs.

Model and its equation		**Parameter**	**Value**
		$q_{e,exp}$	197.98
PFO		$q_{e,cal}$	51.03
$Log(q_e - q_t) = Log(q_e) - \frac{K_{PFO}}{2.303}t$ (4)		K_{PFO}	0.0052
		R^2	0.8285
PSO		$q_{e,cal}$	204.08
$\frac{t}{q_t} = \frac{1}{K_{PSO}q_e{}^2} + \frac{1}{q_e}t$ (5)		K_{PSO}	0.0019
		R^2	0.9996
		K_{IPD1}	16.0461
	1st linear portion	C_1	35.28
		R^2	0.9811
		K_{IPD2}	10.1487
IPD	2nd linear portion	C_2	49.76
$q_t = K_{IPD}t^{1/2} + C$ (6)		R^2	0.9045
		K_{IPD3}	3.1460
	3rd linear portion	C_3	62.75
		R^2	0.9733

529

530

531

532 **Table 3**. TC adsorption isotherm parameters using SiO_2 NPs.

Model and its equation		**Parameter**	**Value**
Langmuir		Q_m	552.48
$\frac{C_e}{q_e} = \frac{1}{Q_m K_L} + \frac{C_e}{Q_m}$	(7)	K_L	0.3175
		R^2	0.9931
Freundlich		K_F	188.7644
$Lnq_e = LnK_F + \frac{LnC_e}{n}$	(8)	n	3.5997
		R^2	0.9650
Temkin		K_T	18.3610
$q_e = BLnK_T + BLnC_e$	(9)	B	75.6710
		R^2	0.9392

533

534

535 **Table 4**. Comparison of TC adsorption onto some adsorbents

Adsorbent	**Ad** (mg L^{-1})	**T** (°C)	***t*** **(min)**	C_0 (mg L^{-1})	**pH**	Q_m (mg g^{-1})	**Reference**
ZrO_2 NPs	0.2	–	15	25–150	6	526.32	(Debnath et al., 2020)
AgO/MgO/FeO@Si_3N_4	–	30	90	30–100	8	172.41	(Sharma et al., 2020)
ACCS	2.5	–	20	100–700	5	38.30	(Song et al., 2020)
ZVI@ACCS	2.5	–	20	100–700	5	78.30	(Song et al., 2020)
NiFe2O4@CDs	10	50	1440	25–100	8	591.72	(Liu et al., 2017)
Pristine MoS_2	0.4	35	2400	50–500	6	409.84	(Li et al., 2021)
NiFe NPs	0.3	–	90	20–80	7	61.00	(Ravikumar et al., 2019)
La_2S_3 NPs	1	25	90	10–300	5	56.81	(Rashidi Nodeh et al., 2020)
SiO_2 NPs	0.25	23	40	25–200	5	552.48	Current study

536

537 **Notation** : Ad=Adsobent dose, T=Temperature, t=Time, C_0= TC concenration

538

539 **Table 5.** ANOVA data for design for TC removal using SiO_2 NPs.

Source	**Sun Squares**	**df**	**Mean Square**	**F-value**	**p-value**
Model	1221.20	9	135.69	162.55	< 0.0001
A-TC concentration	639.35	1	639.35	765.93	< 0.0001
B -Contact time	195.12	1	195.12	233.75	< 0.0001
C- SiO_2 NPs dose	10.72	1	10.72	12.85	0.0043
AB	110.78	1	110.78	132.71	< 0.0001
AC	3.24	1	3.24	3.88	0.0746
BC	0.0406	1	0.0406	0.0487	0.8295
A^2	191.81	1	191.81	229.78	< 0.0001
B^2	83.37	1	83.37	99.88	< 0.0001
C^2	6.39	1	6.39	7.66	0.0183
Residual	9.18	11	0.8347		
Lack of Fit	8.85	5	1.77	31.76	0.0003
Pure Error	0.3343	6	0.0557		
Core total	1230.38	20			
Model statistics	R^2	Adjusted R^2	Predicted R^2	Adequate precision	
	0.9925	0.9864	0.9449	37.9356	

540

541

542

543

544